THE PUBLISHING HOUSE
OF THE ROMANIAN ACADEMY

PROCEEDINGS OF THE ROMANIAN ACADEMY, Series A,
Volume14, Number 4/2013, pp. 351–359

COMPUTATION AND MEASUREMENT OF STRAND CURRENTS IN A FULL-SCALE MULTISTRAND CONDUCTOR

Toma DORDEA[1], Victor PROCA[2], Gheorghe MADESCU[1], Ileana TORAC[1], Marius BIRIESCU[3], Marţian MOŢ[1], Lucian OCOLIŞAN[1]

[1] Romanian Academy, Timişoara Branch, Timişoara, Romania, tdordea@d109lin.upt.ro
[2] ICMET, Craiova, Romania, vproca@icmet.ro
[3] "Politehnica" University, Timişoara, Romania, marius.biriescu@et.upt.ro
Corresponding author: Marţian Moţ, E-mail: martian@d109lin.upt.ro

The paper deals with computation and measurement of strand currents in a full-scale copper bar with non-transposed strands. In this eddy currents problem, the current density distribution within multi-strand conductor are calculated with a numerical method (strips method) and are compared with the measured values using a full scale model bar test setup. The calculated results are close to the measured values of the strand currents and confirm the effectiveness of the "strips method" providing a good estimation of both strand currents and additional losses in multi-strand winding bars (including windings bar with transposed strands) of high power electrical machines.

Key words: eddy currents, numerical method, multistrand bars.

1. INTRODUCTION

The eddy currents are one of the main problem in the field of electrical machines design. The time-varying magnetic field within a conducting material causes eddy currents that flow within the conductor and causes additional and unwanted losses and, in consequences, additional heating. Because temperature rise in stator coils of electrical machines is a major design-limiting factor, it is necessary to minimize the additional copper losses. Minimization of these additional losses within the multi-strand windings is an important goal having as effect the increase of the efficiency of high power electrical machines. Even a small improvement in efficiency of high power machines can give a considerable amount of financial savings. In order to solve this optimization problem it is necessary to estimates all the strand currents.

The eddy currents within a current-carrying conductor lying in a slot, namely current displacement effect ("Field effect") was originally investigated by Field [1] using Poisson equation in the case of an open-type slot, with the assumption that all flux lines go straight across the slot.

Swann and Salmon [2] investigates analytically the more general case of a semi-closed slot and found that "the current density at any point can be expressed in the form of an infinite series of hyperbolic functions, from which the complex impedance per unit length of conductor has been determined". For the particular case of open-type slot the field pattern obtained by Swann and Salmon [2] is precisely of the form assumed by Field, namely that "the flux lines go straight across the slot throughout its depth".

A very interesting formulation of the steady-state skin effect problems is presented by Konrad in [3]. This new method consist of "replacing the diffusion equation containing two unknown quantities (the magnetic vector potential and the source current density vector) with a single integrodifferential equation containing only the unknown magnetic vector potential and the known measurable total current in the conductor". The one-dimensional and two-dimensional finite element discretization of this equation has been treated in some author's work.

Vogt et al. [4, 5] investigates the displacement effect of the current in slot embedded conductors of electrical machines and presents the basic principles of analytical eddy-current losses calculation for single

and multi-strand solid conductors. Vogt suggests also a numerical method for current distribution computation by dividing the solid conductor in many sheets parallel with the bottom of the slot.

The computation methods of circulating currents in multistrand bars (with or without transposition) used in present are based on analytical methods [6] 7] using circuit equations and self and mutual inductances, or finite elements method [8–11], or both analytical and numerical methods [12, 13].

In some previous works [14–16] the authors have been presented more detailed a method for eddy-currents computation within multistrand bar windings of high power electrical machines. This method provide good estimation of the strand currents, taking in to account all the magnetic fields that produce some copper losses and use closed-form analytical relations.

Based on this method, the present paper compares the calculated and measured values of the strand currents of a full-scale model bar with non-transposed strands.

2. THE BASIC ELEMENTS OF THE COMPUTING METHOD

The computation principle of this method is similar with that suggested by Vogt [4] in the case of a rectangular solid conductor embedded in a rectangular open-type slot.

In order to take into account the eddy currents, generally, it is necessary to solve a 3-D problem. In this paper, it is assumed that the eddy currents flow in the axial direction of the conductor. This reason reduces the analysis to a 2-D problem. In this case, under the hypothesis of sinusoidal current carrying conductor, only the **z** – component of the current density phasor $\overline{J}$ and the **y** – component of the magnetic field strength phasor $\overline{H}$ exists according with Fig. 1. Assuming infinite permeability of the iron, the magnetic field strength must be zero everywhere in the iron and at the bottom of the slot; on suppose that all flux lines go straight across the slot in a direction normal to the slot walls.

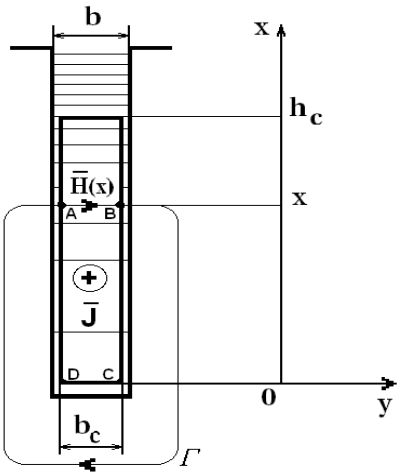

Fig. 1 – Cross-section through a solid conductor embedded in an open slot.

According with this assumptions, the line integral of the magnetic field strength $\overline{H}$, taken around the Γ – curve, is:

$$\oint_{\Gamma} \overline{H} \cdot \mathrm{d}\overline{l} = \int_{S_\Gamma} \overline{J} \cdot \mathrm{d}\overline{s} \ . \tag{1}$$

Because infinite permeability, line integral becomes:

$$\oint_{\Gamma} \overline{H} \cdot \mathrm{d}\overline{l} = b \cdot \overline{H}(x) \ . \tag{2}$$

The current density phasor $\overline{J}$ is different from zero only in the conductor and is dependent only of x-coordinate. Therefore:

$$\int_{S_\Gamma} \overline{J} \cdot \mathrm{d}\overline{s} = \int_{\mathrm{ABCD}} \overline{J} \cdot \mathrm{d}\overline{s} = \int_0^x \overline{J}(x) \cdot b_c \cdot \mathrm{d}x = \overline{I}_u(x). \tag{3}$$

where $\overline{I}_u(x)$ is the total current corresponding to ABCD cross-section and depending only of the x-coordinate.

In consequence, substituting equations (2) and (3) into equation (1), an expression for the magnetic field strength is obtained as:

$$\overline{H}(x) = \frac{1}{b} \int_0^x \overline{J}(x) \cdot b_c \cdot \mathrm{d}x \ . \tag{4}$$

Let us proceed by dividing the solid conductor from Fig. 1 in many strips, numbered from 1 to n, parallel with the bottom of the slot. The number "n" of strips is chosen so as to be justifiably to consider that on the thickness of each strip the current density is constant.

Now, to become clear the principle of the method, in Fig. 2 the strip number $n = 9$ was considered. Along the slot length L, all the strips ν (ν=1, n), have the same thickness h, the same electrical resistance R_ν, but different currents $\overline{I}_\nu$ and different current density $\overline{J}_\nu$. The total current of the solid conductor is $\overline{I}$. The strip currents $\overline{I}_\nu$ (ν=1, n), concentrated in the center of each strip are considered.

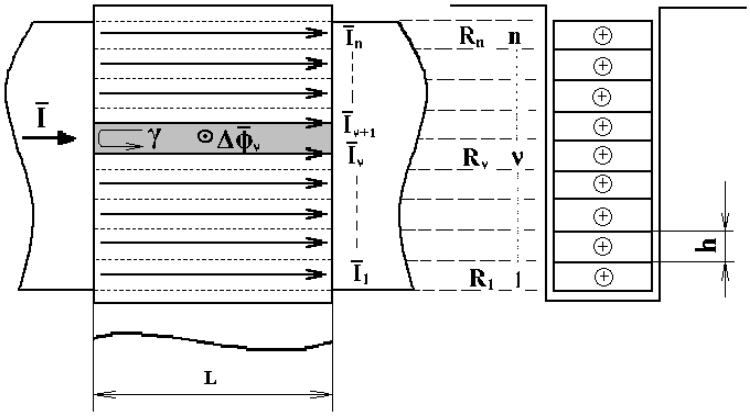

Fig. 2 – Strip currents $\overline{I}_\nu$ into the stranded conductor.

According with electromagnetic induction law, the line integral of electric field strength $\overline{E}$, taken around the γ-curve (boundary line of the dark-surface, in Fig. 2), is:

$$\oint_\gamma \overline{E}\cdot \mathrm{d}\overline{l} = -\frac{\mathrm{d}}{\mathrm{d}t}\int_{S_\gamma} \overline{B}\cdot \mathrm{d}\overline{s}\ , \tag{5}$$

where $\overline{B}$ is the flux density on the dark-surface S_γ.

If we consider the angular frequency ω of the bar current $\overline{I}$, relation (5) becomes:

$$\overline{E}_\nu \cdot L - \overline{E}_{\nu+1}\cdot L = -\mathrm{j}\cdot\omega\cdot\Delta\overline{\Phi}_\nu\ , \tag{6}$$

where $\Delta\overline{\Phi}_\nu$ is the elementary magnetic flux corresponding to surface S_γ.

The terms on the left side of relation (6) represents strip voltage drops along the slot length L, so that $\overline{E}_\nu \cdot L = R_\nu \cdot \overline{I}_\nu$ (ν=1, n).

On the other hand, the elementary magnetic flux can be formulated as:

$$\Delta\overline{\Phi}_\nu = \overline{B}_\nu \cdot L\cdot h = \mu_0\cdot\overline{H}_\nu\cdot L\cdot h = \mu_0\cdot L\cdot h\cdot\frac{1}{b}\cdot\sum_{k=1}^{\nu}\overline{I}_k\ , \tag{7}$$

where the relation (4) was considered.

In consequence, the relation (6) becomes:

$$R_\nu\cdot\overline{I}_\nu - R_{\nu+1}\cdot\overline{I}_{\nu+1} = -\mathrm{j}\cdot\omega\cdot\mu_0\cdot L\cdot h\cdot\frac{1}{b}\cdot\sum_{k=1}^{\nu}\overline{I}_k\ , \tag{8}$$

Because all the strips have the same thickness h, we can write:

$$R_1 = R_2 = \ldots = R_\nu = \ldots = R_n = \rho\cdot\frac{L}{b_c\cdot h}\ . \tag{9}$$

Substituting relation (9) into relation (8), finally, a recursion formula for the strip current is obtained as:

$$\overline{I}_{\nu+1} = \overline{I}_\nu + \mathrm{j}\cdot\omega\cdot\mu_0\cdot\frac{h^2\cdot b_c}{\rho\cdot b}\cdot\sum_{k=1}^{\nu}\overline{I}_k\ . \tag{10}$$

Only (n – 1) such relations can be written for all the n strips. In addition, it is now evident that we may consider another one simple relation:

$$\sum_{k=1}^{n} \bar{I}_k = \bar{I} . \tag{11}$$

Based on relations (10) and (11), all the strip currents $\bar{I}_\nu$ (ν=1, n) can be computed.

This computation principle of the strip currents and strand currents into the multistrand conductor of the winding bars of high power machines was applied also in order to estimate finally the additional copper losses of bar windings with transposition strands. Many details about the method in the case of bars with transposition strands in [14–16] may be find.

In what follows we presents the computed results obtained with this method and measured values of the strand current in a stranded full-scale bar with nontransposed strand in order to validate the method. Such test results and comparative results also in the paper [17] was presented

3. FULL-SCALE MODEL BAR TEST SETUP

In this chapter, we shortly presents the specifications of the full-scale model bar tests setup used for strand currents measurement.

The model bar has 28 parallel-connected non-transposed copper strands (Fig. 3) in order to produces a strong skin effect and very different strand currents in the case of slot-embedded bar.

The measurement results were used to validate the proposed method of strand currents computation.

Each strand of the bar has one's own transducer that allows to measure the strand current (Fig. 4). Therefore, it is possible to known the currents distribution on the bar cross-section.

1	28
2	27
3	26
4	25
5	24
6	23
7	22
8	21
9	20
10	19
11	18
12	17
13	16
14	15

Fig. 3 – The stranded bar structure with 28 non-transposed strands.

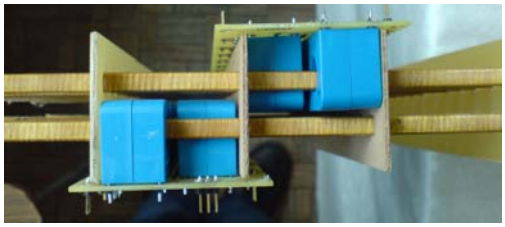

a) Top view.

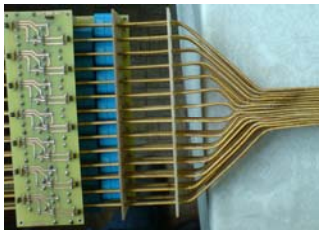

b) Lateral view.

Fig. 4 – Model bar with current transducers mounted on each strand.

The experimental test setup is shown in Fig. 5. One can be see two bars embedded in the core slot. The iron core is made with iron sheets of 0.5 mm thickness. The bar dimensions corresponds to the hydro-generator of 22 MVA working in a actual Romanian power plant.

Other technical specifications and geometrical dimensions are given in Table 1.

Table 1

Specifications of the experimental model

Length of iron core [mm]	900
Total bar length [mm]	2000
Slot width [mm]	20
Slot height [mm]	100
Bar cross-section [mm^2]	42.2 x 19.1
Strand cross-section [mm^2]	6.3 x 2.5
Strands number	28
Transducer type	LEM HTY 75P

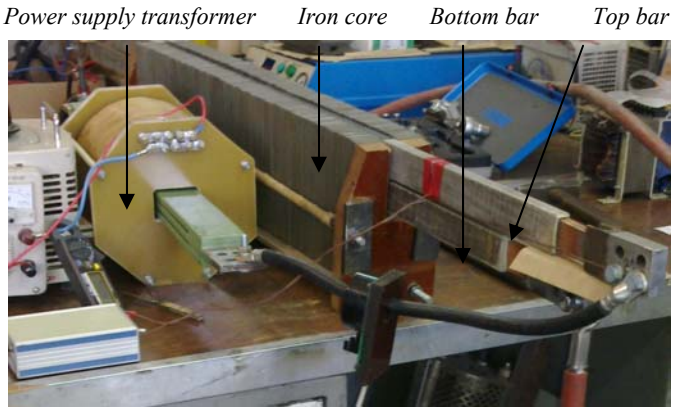

Fig. 5 – Photo of full-scale model bar test setup.

4. CALCULATED AND MEASURED RESULTS

The tests and computations were made on the model bar in three different conditions in order to simulate different kind of skin effects. First, the bar is placed in free space, when arise a soft skin effect. Second, the bar is embedded in the slot (single layer and double layer) when the skin effect is very strong.

4.1. Model bar in free space

Firstly, based on the strips method, the strand currents of the bar were calculated in the case when the bar was placed in free space. The total bar current was fixed at 492 A (rms value), at 50 Hz.

The calculated strand currents as complex phasors (rms) are given in Table 2.

These strand currents as phasor diagram and hodograph curve are shown in Fig. 6.

Table 2

Calculated strand currents (free space)

Strand No.	Current phasor [A]	Modulus [A]
1; 28	19.0045 + 7.5310 j	20.4423
2; 27	17.0043 + 8.5111 j	19.0154
3; 26	18.3962 + 0.6766 j	18.4086
4; 25	17.8321 – 1.8583 j	17.9286
5; 24	17.2988 – 3.7918 j	17.7095
6; 23	16.8689 – 5.1424 j	17.6353
7; 22	16.5953 – 5.9263 j	17.6217
8; 21	16.5953 – 5.9263 j	17.6217
9; 20	16.8689 – 5.1424 j	17.6353
10; 19	17.2988 – 3.7918 j	17.7095
11; 18	17.8321 – 1.8583 j	17.9286
12; 17	18.3962 + 0.6766 j	18.4086
13; 16	17.0043 + 8.5111 j	19.0154
14; 15	19.0045 + 7.5310 j	20.4423

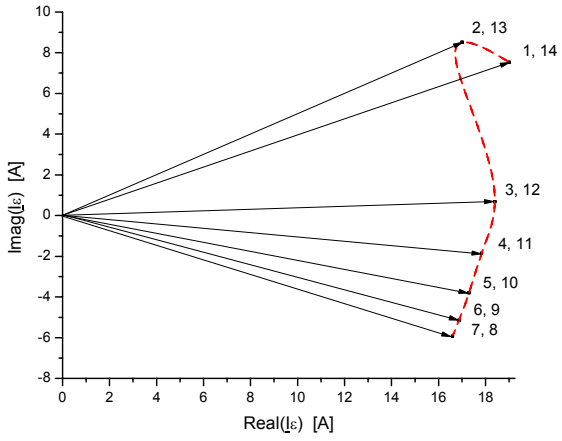

Fig. 6 – Phasor diagram of calculated strand currents and hodograph curve.

The test results representing the strand currents distribution (28 strand currents) in model bar placed in free space are shown in Fig. 7.

The tests were made with a total bar current of 492 A (rms value), at 50Hz.

The calculated and measured values in these conditions are compared in Fig. 8. As shown in this figure there is some unsymmetrical current distribution in test results because, after test, we see some unsymmetrical permeability conditions in free space around the bar.

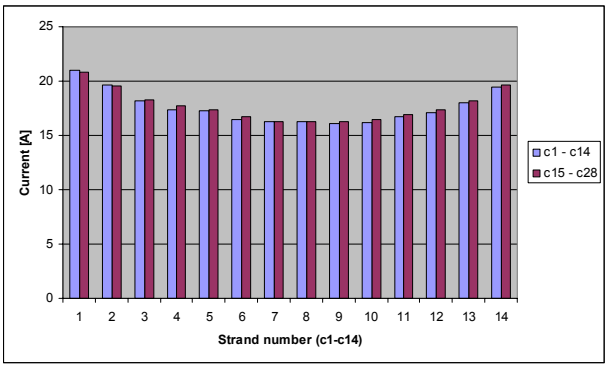

Fig. 7 – Measured strand currents distribution in the model bar in free space (492 A).

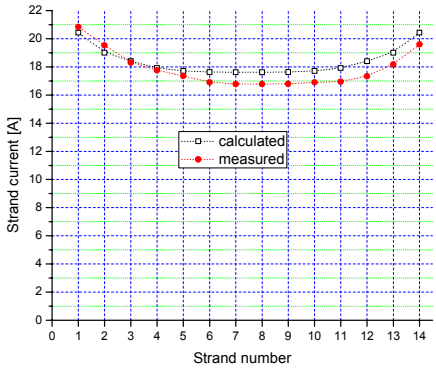

Fig. 8 – Measured and calculated strand currents distribution in free space (492 A).

4.2. Slot embedded bar – single layer

In this case, the model bar is embedded in the slot (top position) without current in bottom bar (Fig. 5). The calculated strand currents as complex phasors are given in Table 3.

The phasors diagram and hodograph curve of the strand currents are shown in Fig. 9. This phasor diagram (Fig. 9) is very close to the phasor diagram for the voltage drops per unit length in an elemental filament determined by Swann (Fig. 5 in [2]).

Table 3

Calculated strand currents (slot embedded bar)

Strand No.	Current phasor [A]	Modulus [A]
1; 28	38.3947 + 34.1789 j	51.4039
2; 27	36.2900 + 23.8236 j	43.4112
3; 26	34.3752 + 12.6615 j	36.6329
4; 25	30.5942 + 5.0139 j	31.0024
5; 24	26.3541 – 0.7890 j	26.3659
6; 23	22.0306 – 4.9905 j	22.5888
7; 22	17.9016 – 7.8463 j	19.5457
8; 21	13.6601 – 8.7083 j	16.1998
9; 20	10.4272 – 9.5831 j	14.1620
10; 19	7.7256 – 9.8349 j	12.5064
11; 18	5.5843 – 9.6370 j	11.1381
12; 17	4.0045 – 9.1313 j	9.9708
13; 16	2.7470 – 8.5461 j	8.9767
14; 15	2.4091 – 7.6100 j	7.9823

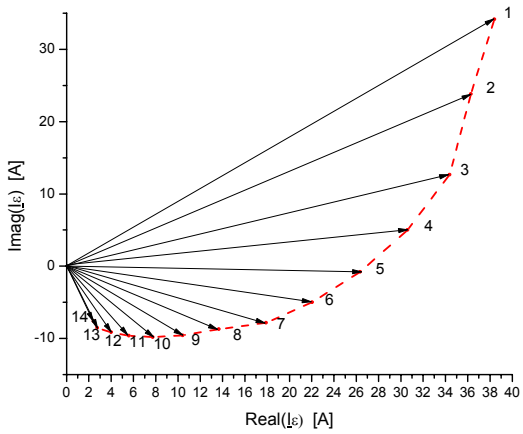

Fig. 9 – Phasor diagram of calculated strand currents and hodograph curve in the case of slot embedded bar (total current 505 A, rms).

Experimental recorded values of the strand currents in the slot embedded single bar using data acquisition system are shown in Fig. 10. Because the system has 16 channels, were recorded at a given moment all strand currents of first column (c1-c14) and another two strand currents of second column (c26 and c27). As we can see in Fig. 10 the strand current c2 and c27, or c3 and c26 are very close each other.

The test results representing the modulus of the strand currents distribution in slot embedded bar are shown in Fig.11.

The tests were made with a total bar current of 505 A (rms value), at 50Hz. Without skin effect (d.c. – conditions) all the strand currents will be equal with 18.036 A.

The calculated and measured values of the strand currents are compared in Fig. 12.

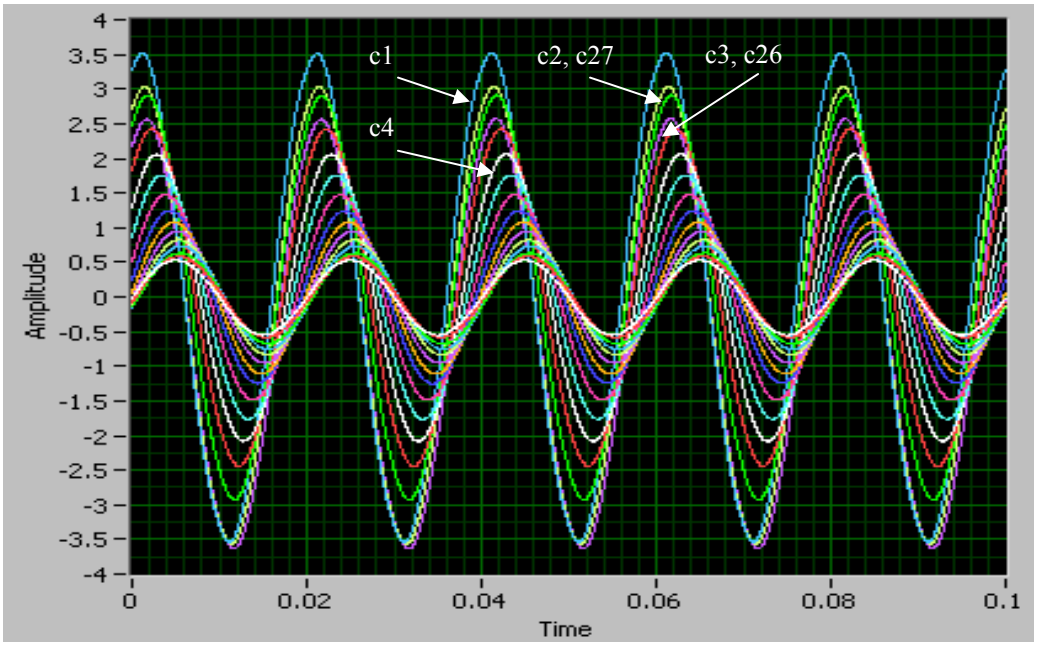

Fig. 10 – Measured time variation of the strand currents in the slot embedded single bar.

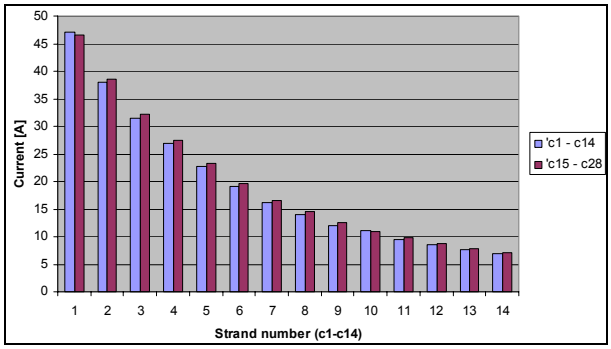

Fig. 11 – Measured strand currents distribution in the single model bar embedded in the slot (total bar current 505 A).

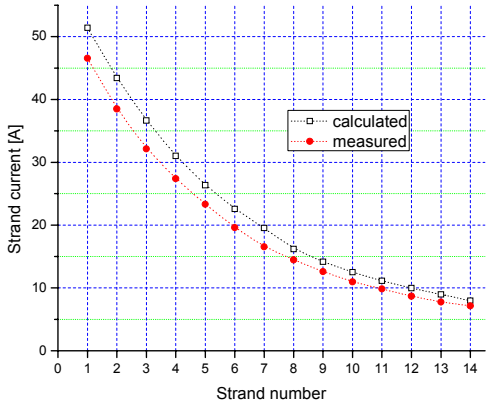

Fig. 12 – Measured and calculated strand current distribution in slot embedded bar (total bar current 505 A).

4.3. Slot embedded bar – double layers

In what follows, we consider the case in which the model bar (top position) is connected in series with bottom bar and is carried by a.c. current (381 A, rms, 50 Hz). For this case, Table 4 contain calculated strand currents as complex phasors.

These calculated currents as phasors diagram and hodograph curve are shown in Fig. 13.

The test results representing the strand current distribution in top bar (double layers) are shown in Fig. 14.

The calculated and measured values of the strand currents in top bar are compared in Fig. 15.

Some test recorded currents in the strands of the top bar are given in Fig. 16. The neighbor strand currents (c1, c28, or c2, c27, and so on) are very close each other as can be see in Fig. 16b.

As we have seen so far (Fig. 8, Fig. 12, Fig. 15) the calculated strand currents are overestimated because the strips method was developed assuming that the magnetic field lines in the slot are parallels to the slot basis (and also infinite permeability of iron) that cause a stronger skin effect that real cases. On the other hand, a little overestimated strand currents or copper losses are favorable, representing a good assurance and not disturb an optimization process of bar structure.

Table 4

Calculated Strand Currents (Slot Embedded Bar)

Strand No.	Current phasor [A]	Modulus [A]
1; 28	54.8275 + 57.6247 j	79.5403
2; 27	51.6112 + 41.8819 j	66.4667
3; 26	48.1615 + 25.7412 j	54.6090
4; 25	41.5761 + 14.2566 j	43.9525
5; 24	33.8992 + 5.3459 j	34.3181
6; 23	25.7063 – 1.4248 j	25.7457
7; 22	17.4377 – 6.5330 j	18.6214
8; 21	8.2959 – 8.5594 j	11.9200
9; 20	0.7530 – 11.8212 j	11.8452
10; 19	– 6.1861 – 14.9365 j	16.1669
11; 18	– 12.3370 – 18.3339 j	22.0983
12; 17	– 17.5051 – 22.6006 j	28.5870
13; 16	– 21.2556 – 27.0273 j	34.3843
14; 15	– 23.9459 – 33.8094 j	41.4305

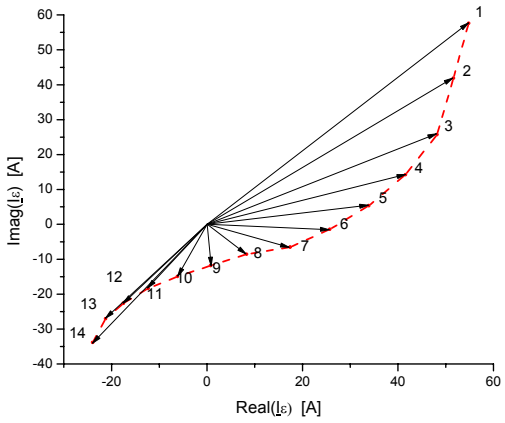

Fig. 13 – Phasor diagram of calculated strand currents and hodograph curve in top bar (double layer, 381 A, rms)..

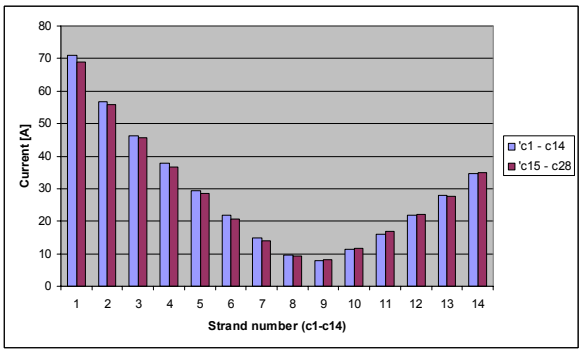

Fig. 14 – Measured strand currents distribution in top bar (381 A, rms, 50 Hz)

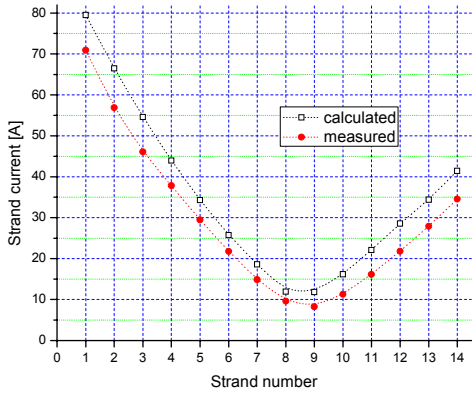

Fig. 15 – Measured and calculated strand currents distribution in top bar (381 A, rms, 50 Hz).

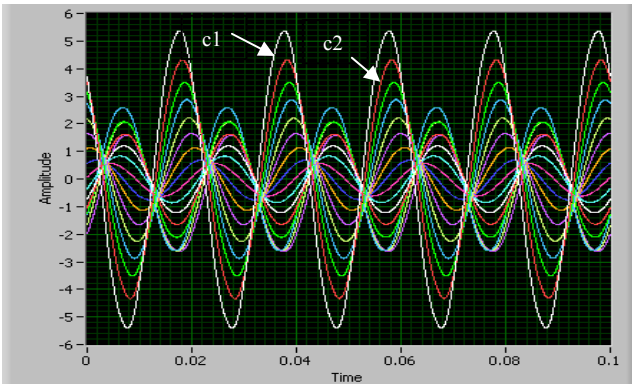

a) Strand currents c1, c2, c3, …c14.

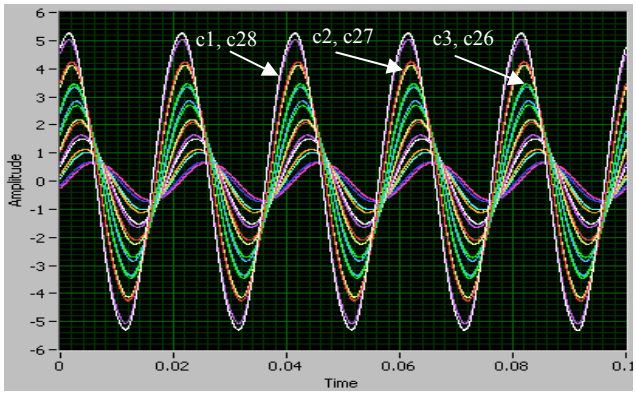

b) Strand currents c1,…c8, and c21,…c28.

Fig. 16 – Measured time variation of some strand currents in top bar (381 A, rms, 50 Hz).

5. CONCLUSIONS

This paper deals with analysis of strand currents distribution in a stranded bar with non-transposed strand. The currents distribution are calculated with a computing program based on a numerical method ("strip method") presented in details in few previous papers. This program allows a faster analyze of the

strand currents distribution and, if is necessary, can provide an optimal bar structure (with or without transposition) that means a minimum additional copper bar losses.

The calculated strand currents are compared in the paper with measured values using a full-scale model bar test setup in order to validate the computing method.

The calculated results are close to the measured values of the strand currents and confirm the effectiveness of the strips method that provides a good estimation of both strand currents and additional losses in winding bars (including Roebel bars) of high power electrical machines.

In addition, this numerical method allows in-depth study and gives greater insight into the problem of skin effect in current-carrying conductors.

REFERENCES

1. A. B. Field, *Eddy currents in large slot-wound conductors*, T.A.I.E.E. 1905, 24, p.761.
2. S. A. Swann, J. W. Salmon, *Effective resistance and reactance of a rectangular conductor placed in a semi-closed slot*, Proc. IEE, **110**, *9*, pp. 1656–1662, 1963.
3. A. Konrad, *The numerical solution of steady state skin effect problems – An integrodifferential approach*, IEEE Trans. on Magnetics, **Mag-17**, *1*, January, pp. 1148–1152, 1981.
4. K. Vogt, *Elektrische Maschinen. Berechnung Rotierender elektrischer Maschinen*, Veb Verlag Technik, Berlin, 1974.
5. G. Muller, K. Vogt, B. Ponik, *Berechnung elektrischer Maschinen*, Wiley – VCH Verlag, 2008.
6. K. Takahashi, K. Ide, M. Onoda, K. Hattori, M. Sato, M. Takahashi, *Strand Current Distribution of Turbine Generator Full-Scale Model Coil*, Proc. of ICEM 2002, Brugge, Belgium, 25–28 August 2002.
7. Haldemann, J., *Transpositions in Stator Bars of Large Turbo-generators*, IEEE Transactions on Energy Conversion, **19**, *3*, pp. 553–560, 2004.
8. Chari, M.V.K., Csendes, Z.J., *Finite element analysis of the skin effect in current carrying conductors*, IEEE Trans. on Magnetics, **13**, *5*, pp. 1125–1127, 1977.
9. Preis, K., Bardi, I., Biro, O., Richter, K.R. 1996. *Nonlinear periodic eddy currents in single and multi-conductor systems*, IEEE Trans. on Magnetics, **32**, *3*, pp. 780–783, 1996.
10. Arshad, W.M., Lendenmann, H., Persson, H. 2008. *End-winding inductances of MVA machines through FEM computations and IEC-specified measurements*, IEEE Trans. on Industry Applications, **44**, *6*, pp. 1693–1700, 2008.
11. M. J. Islam, *Finite-element analysis of eddy currents in the form-wound multi-conductor windings of electrical machines*, ESPOO, 2010, TKK Dissertation 211, Helsinki University of Technology.
12. A. Schwery, G. Traxler-Samek, E. Schmidt, *Numerical and Analytical Computation Methods for the Refurbishment of Hydro-Generators*, Proc. of ICEM 2002, Brugge, Belgium, 25–28 August 2002.
13. M. Fujita, Y. Kabata, T. Tokumasu, K. Nagakura, M. Kakiuchi, S, Nagano, *Circulating currents in stator coils of large turbine generators and loss reduction*, IEEE Trans. on Industry Applications, **45**, *2*, pp. 685–693, 2009.
14. Dordea T., Biriescu M., Madescu G., Torac I., Moţ M., Ocolişan L. *Calcul des courents electriques par les conducteurs elementaires d'une barre Roebel. Part I: Fondements de calcul*, Rev. Roum. Sci. Techn. – Électrotechn. et. Énerg., **48**, *2–3* pp. 359–368, 2003.
15. Dordea T., Biriescu M., Madescu G., Torac I., Moţ M., Ocolişan L., *Calcul des courents electriques par les conducteurs elementaires d'une barre Roebel. Part II: Détermination des courents*, Rev. Roum. Sci. Techn. – Électrotechn. et. Énerg., **49**, *1*, pp. 3–29, 2004.
16. Dordea T., Câmpean A., Madescu G., Torac I., Moţ M, Ocolisan L, *Strips Method For Evaluating AC Losses in Slot Portion of Roebel Bars - Errors Analysis*, Rev. Roum. Sci. Tech. – Electrotech.et Energ., Bucarest, **54**, *1*, pp. 29–36, 2009.
17. Dordea T., Proca V., Madescu G., Torac I., Biriescu M., Moţ M., Ocolişan L., *Current distribution analysis in nontransposed elementary conductors of a full scale model bar*, 13th International Conference on Optimization of Electrical and Electronic Equipment – OPTIM 2012, May 24–26, 2012, Braşov, Romania.

Received July 2, 2013